Research Article Vol. 8, No. 9 / September 2021 / Optica 1153

optica

Phonon dephasing and spectral diffusion of quantum emitters in hexagonal boron nitride

Simon White,[1] Connor Stewart,[1] Alexander S. Solntsev,[1] Chi Li,[1] Milos Toth,[1,2] Mehran Kianinia,[1,2,*] and Igor Aharonovich[1,2]

[1]School of Mathematical and Physical Sciences, Faculty of Science, University of Technology Sydney, Ultimo, New South Wales 2007, Australia
[2]ARC Centre of Excellence for Transformative Meta-Optical Systems (TMOS), University of Technology Sydney, Ultimo, New South Wales 2007, Australia
*Corresponding author: Mehran.kianinia@uts.edu.au

Received 12 May 2021; revised 23 July 2021; accepted 25 July 2021 (Doc. ID 431262); published 26 August 2021

Quantum emitters in hexagonal boron nitride (hBN) are emerging as bright and robust sources of single photons for applications in quantum optics. In this work we present detailed studies on the limiting factors to achieve Fourier transform limited spectral lines. Specifically, we study phonon dephasing and spectral diffusion of quantum emitters in hBN via resonant excitation spectroscopy at cryogenic temperatures. We show that the linewidths of hBN quantum emitters are phonon broadened, even at 5 K, with typical values of the order of ∼1 GHz. While spectral diffusion dominates at increasing pump powers, it can be minimized by working well below saturation excitation power. Our results are important for future utilization of quantum emitters in hBN for quantum interference experiments.

https://doi.org/10.1364/OPTICA.431262

1. INTRODUCTION

Solid-state quantum light sources are emerging as promising candidates for many applications in quantum technologies [1–3]. Among these sources, optically active point defects in hexagonal boron nitride (hBN) are attracting considerable attention due to their extreme brightness, and high Debye–Waller factor, which means the majority of the photons are emitted into the zero phonon line (ZPL) [4–8]. While final defect assignments are still under debate [9], a number of recent experiments and theoretical papers hint at carbon-related defects adjacent to a vacancy site in the hBN lattice [10,11]. In addition, numerous recent studies have shown that several defects in hBN exhibit spin-dependent optical transitions and exhibit optically detected magnetic resonance (ODMR), which is vital for their employment as solid-state qubits and quantum sensors at the nanoscale [12–14].

For practical quantum photonic applications, where photon interference and generations of indistinguishable photons are required [15–18], it is important to characterize the coherent properties of the emitted photons. Specifically, studies of dephasing mechanisms [19,20], coherence, and line broadening effects underpin the applicability of quantum emitters for photon interference experiments. Previous studies of hBN quantum emitters have revealed that the emissions in hBN are broadly affected by spectral diffusion [21–27]. Preliminary resonant excitation experiments showed that observation of Fourier transform limited lines is possible but rather rare [27] as compared to other solid state emitters such as diamond [28,29]. Some of the challenges stemmed from the fact that the level structure of the emitters is still poorly understood, and environmental effects in layered materials are strongly sample dependent.

In this work, we employ coherent excitation spectroscopy at cryogenic temperatures to study the dephasing of quantum emitters in hBN. Importantly, our work focuses predominantly on coherent excitation (i.e., the excitation laser is on-resonance with the hBN emission). We find that even at low temperatures of 5 K, the lines are predominantly broadened by phonon coupling. We also observe that spectral diffusion can be minimized by employing excitation powers well below the saturation power. We explain our results in the context of electron–phonon coupling and provide an important analysis for future experiments on two-photon interference with quantum emitters in hBN.

The hBN flakes were mechanically exfoliated onto a silicon substrate from high-purity bulk hBN. The exfoliated hBN flakes were then treated with a H_2 plasma (10 min at 900 W, 100 sccm at 60 torr), after which the sample was annealed for 30 min in air at 850°C to remove any residual contaminants from the hBN surface. The sample was then placed under vacuum in a closed-loop cryostat and cooled to 5 K.

2. RESULTS

The main dephasing mechanisms of the hBN emitters are shown in Fig. 1(a). Coupling to lattice phonons (phonon dephasing) and random fluctuations of trapped charges in close proximity to the defect (spectral diffusion) are the main dephasing processes for all emitters in solid-state hosts that result in broadening of the emission lines. To investigate a particular defect, we screen for

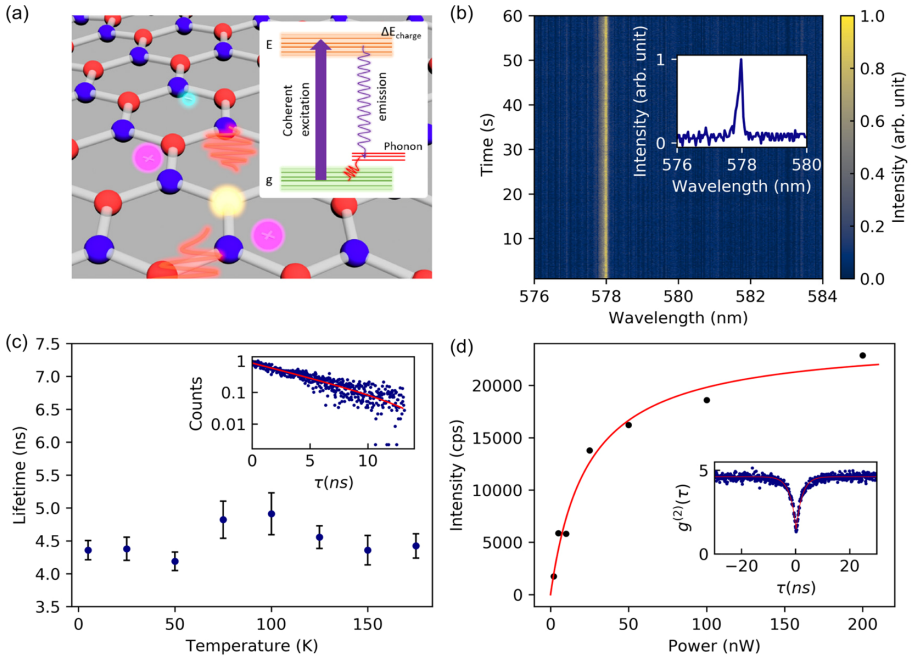

Fig. 1. Characterization of hBN single-photon emitters. (a) Schematic representation of the hBN lattice with a point defect (yellow sphere). The emission from the defect is broadened by charge fluctuations and lattice phonons. The inset is a simplified electron energy diagram that illustrates dephasing pathways under resonant excitation. (b) PL spectra of hBN emitters under 532 nm excitation at 5 K. Each spectrum was recorded for 0.1s. The inset is a single PL spectrum of the same emitter. (c) hBN SPE lifetime showing no significant change versus temperature, under 512 nm pulsed excitation. Error bars are uncertainty of the fit (95% confidence interval). The inset demonstrates a representative lifetime measurement acquired at 5 K. The red line is a single exponential fit of the data. (d) PL saturation measurement of the hBN emitter under resonant excitation. The inset shows a resonant $g^2(\tau)$ measurement, recorded under 10 nW excitation power.

a relatively bright emitter with spectrometer limited linewidth (<0.1 nm). Figure 1(b) shows the photoluminescence (PL) spectra of such an hBN emitter at 5 K under 1 mW excitation. The emitter does not exhibit any noticeable spectral diffusion as is illustrated by the time series of PL spectra collected over a period of 60s. Next, we used a 512 nm pulsed laser with a repetition rate of 40 MHz to measure the lifetime of the emitter at temperatures in the range of 5 K to 150 K. Figure 1(c) shows that the emission decay rate is approximately constant over this temperature range. The total decay rate from the excited states, $\gamma = 1/\tau_0 = \gamma_r + \gamma_{nr}$, is, in general, a combination of temperature-independent radiative rate (γ_r), and a nonradiative rate (γ_{nr}), which depends on temperature. The dependence of the lifetime on temperature is typically described by the Mott–Seitz model for nonradiative relaxation, $\tau_0(T) = \tau_0(0)\ (1 + a\ \exp[-\Delta E/k_B T])^{-1}$, where ΔE is the activation energy, a is the nonradiative relaxation strength parameter, and k_B is the Boltzmann constant [30]. Our results suggest that nonradiative relaxation in hBN is not affected by phonons, at least within this temperature range [Fig. 1(c)]. A lifetime of 4.4 ± 0.1 ns was derived by fitting a single exponential to the data as shown in the inset of Fig. 1(c). This indicates a Fourier transform limited linewidth of $\sim$ 36 MHz at 5 K from this emitter.

We next coherently excited the emitter by tuning a narrowband laser (linewidth $<$ 100 kHz) to the emission energy of the emitter. For this measurement, the emissions into the phonon sideband were collected using a long-pass filter. First, we measured the saturation behavior of the emitter under resonant excitation as shown in Fig. 1(d). The solid line is a fit to the data with the equation $[I = I_{sat}\ p/(p + P_0)]$, yielding a saturation power of $P_0 = 23.4$ nW and saturation intensity of $I_{sat} = 24.5$ kHz for this emitter. We recorded an autocorrelation curve from the emitter under 10 nW excitation power as shown in the inset of Fig. 1(d). Note that we did not observe Rabi oscillations under excitation powers as high as 10 μW (i.e., well above saturation), indicating strong dephasing faster than the lifetime of the emission [22].

Next, we turn our attention to characterization of the dephasing processes of this emitter, employing the resonant photoluminescence excitation (PLE) scheme. The PL intensity of the resonant excitation under a pump power of 7 nW is shown in Fig. 2(a) fitted with Gaussian and Lorentzian functions (top part of the plot). The Lorentzian function fits better and has substantially lower residuals compared to the Gaussian fit [Fig. 2(a) bottom panels]. A Lorentzian shape indicates that the emission linewidth is homogeneously broadened, and thus phonons are the dominant broadening mechanism even at $\sim$ 5 K. The full width half-maximum (FWHM) of the PLE spectrum in this case is 1.10 ± 0.04 GHz, which is significantly broader than the Fourier transform limited linewidth of 36 MHz estimated from the lifetime of the same emitter (see Fig. 1). Given this linewidth, we would expect to see around 3% of photons to be emitted coherently, resulting in a rather low probability to observe indistinguishable photons (Hong–Ou–Mandel experiment). Note that the saturation measurements were recorded using phonon sideband collection. Under a cross-polarization scheme [31], where ZPL photons can be collected, a much higher count rate of coherent photons is expected. Further improvement in collection of photons from the ZPL can be achieved employing a dielectric cavity.

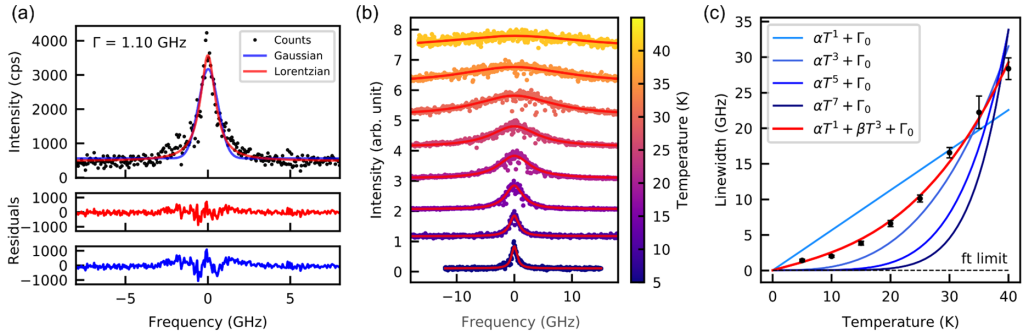

Fig. 2. Phonon-limited linewidth of hBN SPE. (a) Photoluminescence excitation (PLE) spectrum for hBN single-photon emitter. The linewidth is fit with Gaussian and Lorentzian functions (top), with the corresponding residuals for each fit shown in the bottom panels. The Lorentzian fit is closest to the data and reveals a linewidth (FWHM) of $1.10 + -0.04$ GHz at 5 K. (b) Broadening of the emission linewidth is demonstrated as a function of temperature, due to increased interaction with phonons. Each spectrum is fitted with a Lorentzian function (solid red lines). (c) PLE linewidths (FWHM) as a function of temperature, with an error of 1 standard deviation from each Lorentzian fit. A model (solid red), which is a combination of T^1 and T^3, fits experimental data better than the other higher-order polynomial fits. The fit limit (dash line) is set according to the Fourier transform limited linewidth of 36 MHz.

To explore the phonon-related PLE spectral broadening further, we show PLE spectra collected using a relatively low pump power of 7 nW over a temperature range of 4 to 40 K in Fig. 2(b). The emission linewidth increases dramatically as the temperature rises, reaching nearly 30 GHz at 40 K, due to an increase in the interaction rate with phonons. We note that phonon broadening is still the dominant broadening mechanism over this temperature range, which we attribute to the relatively small corresponding change in thermal energy and hence a weak effect on spectral diffusion. As expected, each spectrum shows a nearly perfect fit with a Lorentzian function as shown in Fig. 2(b).

In Fig. 2(c), we plot the PLE FWHM linewidth against the sample temperature and fit the data with $a\,T^1$, $a\,T^3$, $a\,T^5$, $a\,T^7$, and $a\,T + b\,T^3$ curves [30,32,33]. As can be seen from the fittings, higher-order polynomials do not fit as well as $a\,T + b\,T^3$. Closer to absolute zero, the dependence of the linewidth on the temperature is expected to be linear as a first-order approximation [34]. Since we are performing the measurements in the intermediate temperature range, a polynomial fit $a\,T + b\,T^3$ corresponds to the appropriate model. Above 20 K, the linewidth scales as the cube of the temperature $\Gamma = (36 + 0.32 \pm 0.02 \cdot [T]^3)$ MHz. For low temperatures (<20 K), the behavior deviates from T^3 and is better approximated by a linear dependence on temperature $\Gamma = (36 + 220 \pm 29 \cdot [T])$ MHz.

To speculate about the type of the observed electron–phonon interactions and their relation to strain, we note that for defects under strain that is larger than the spin–orbit interaction, the orbital eigenstates no longer have well-defined angular momentum. In that case, the inelastic Raman process results in a competing orbital relaxation rate and the corresponding linewidth dependence on temperature that scales as T^5, which we do not observe in our measurement in hBN defects. The fits with higher-order polynomials T^5 and T^7 do not match our data well, which indicates that in our system degenerate electronic states are not dominant, the Jahn–Teller effect is small, the effect of strain is low, and the inelastic Raman process is not prominent [30,35,36]. When it comes to the type of phonons in the electron–phonon interactions, the linear component of the linewidth temperature dependence corresponds to the first-order transition between the orbital states and the absorption or emission of a single E phonon, while T^3 dependence is related to a two-phonon elastic scattering dephasing process. This phonon broadening effect indicates that further cooling (below 4 K) would enable further narrowing and may enable Fourier transform limited linewidth for such SPEs in hBN. Note that, unlike the situation with single molecules [19], where low energy phonons are visible and present as sharp spectral lines, hBN defects do not exhibit this phenomena, at least at 4 K. Hence the phonons are likely a mixture of bulk and acoustic phonons within the hBN lattice.

Next, we explore the dependence of the PLE emission as a function of pump power at 5 K to evaluate the spectral diffusion of the emitter. Figure 3(a) shows a series of eight individual scans at pump power of 100 nW, which results in a significant spectral diffusion. At the bottom of Fig. 3(a), the integrated spectrum is shown and has a broadened linewidth of ∼ 10 GHz. On the other hand, Fig. 3(b) shows that when the power is reduced to 3 nW the spectral diffusion is significantly reduced to sub-gigahertz (GHz) level.

This measurement is consistent with the temperature-dependent measurements, which show that the linewidth, at a pump power of 7 nW, is broadened due primarily to interactions with phonons and to a lesser extent by spectral diffusion. Interestingly, we also note that the linewidth for individual scans maintains a similar linewidth to the low power scans (∼ 1 GHz), signifying that the dominant broadening mechanism of the line is still homogeneous. This also opens the possibility that active field modulation, post-selection technique, or charge depletion may play a role in enabling bright coherent emission from such hBN source [37,38]. By efficient decoupling of the emitter from its local environment, one could avoid spectral diffusion and enable high-power excitation and emission [38,39].

To reveal the full spectral diffusion behavior of the emitter, we recorded number of PLE scans using excitation powers from 3 to 210 nW as shown in Fig. 3(c). Spectral diffusion is seen to significantly increase at a transition power around 30–65 nW, which corresponds with the saturation power, and stable coherent excitation becomes difficult. These results demonstrate that to use such hBN emitters for quantum interference and enable viable levels of indistinguishability between consecutive photons, it is essential to use excitation powers below saturation and/or lower temperatures.

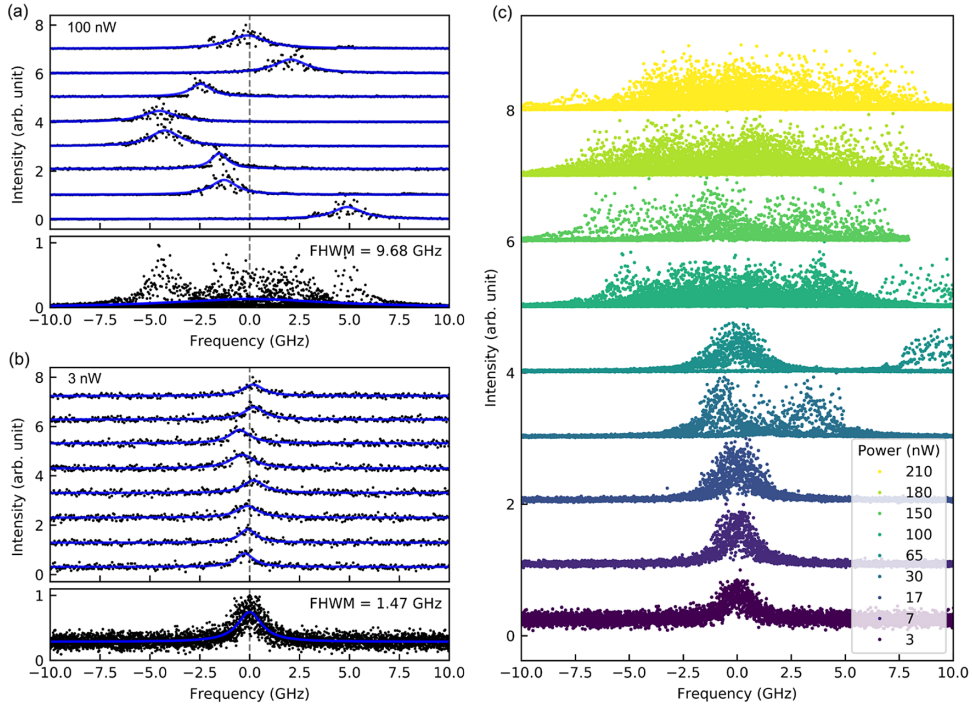

Fig. 3. Power-dependent spectral diffusion characterized by PLE spectroscopy. (a) Individual PLE scans at a pump power of 100 nW (top) and the corresponding integrated PLE spectrum (bottom) showing significant spectral diffusion. (b) Individual PLE scans at a pump power of 3 nW (top) and the corresponding integrated PLE spectrum (bottom) showing negligible diffusion (c) Integrated PLE spectra at pump powers in the range of 3 to 210 nW, showing that the integrated linewidth increases with pump power.

3. CONCLUSIONS

To summarize, in this study we characterize the significant dephasing and spectral broadening mechanisms in an hBN single-photon emitter under resonant excitation. We find that the resonant linewidth, even at cryogenic temperatures, is dominated by phonon broadening and results in linewidths of ~ 1 GHz. The best fit to data indicates that degenerate electronic states and strong strain do not appear to play a significant role in phonon dephasing. We further showed that spectral diffusion can be minimized by employing excitation powers well below saturation.

The work opens exciting opportunities for quantum interference experiments with defects in hBN. Development of cross-polarization schemes to collect ZPL photons should be implemented using waveguide structures [40–43]. This is certainly within reach with the currently available nanofabrication techniques and will enable substantially more photons. Our results also infer that extended cooling below 4 K can enable further narrowing of the spectral linewidth and may enable an approach to generate indistinguishable photons on demand. Finally, established tuning techniques [44,45] can be utilized to not only stabilize spectral diffusion but tune two distinct hBN emitters into same resonance, thus paving way to generation of remote indistinguishable photons.

APPENDIX A

1. Sample Preparation

The hBN used in this work was exfoliated from high crystal bulk hBN and then transferred to SiO_2/Si substrate with a polydimethylsiloxane (PDMS) stamp. A pre-annealing of 500°C is conducted to remove the transfer residuals. The sample is then etched for 10 min in 900 W hydrogen plasma at 60 torr using a microwave plasma deposition system (SEKI AX5100) to create defects on the flake surface. Finally, the sample was annealed for 30 min in a tube furnace (Lindberg/Blue M) in air.

2. Optical Measurement

The sample was mounted on the cooling stage of an Attocube Attodry800 closed-system cryostat, placed under vacuum, and cooled to 4.5 K. Optical measurements were then performed using a custom scanning confocal microscope with a 0.82 NA vacuum compatible objective mounted inside the cryostat (also at 4.5 K). A tunable dye laser (Sirah Matisse 2 DS) with linewidth around 100 kHz was used for resonant excitation, and a 532 nm diode laser (Laser Quantum GEM) was used for off-resonant excitation. For photoluminescence excitation measurements, a scan rate of 1 GHz/s was used to tune the dye laser wavelength over the ZPL, and then the phonon sideband emission from SPE was filtered using a 580 nm longpass filter, coupled via a single-mode fiber, and detected using an Avalanche Photodiode (Excelitas SPCM-AQRH). Second-order correlation measurements were performed using a fiber beam splitter and a TimeTagger20, and lifetime measurements were taken using 40 MHz pulsed 512 nm laser (PiL051X, Advanced Laser Diode Systems GmbH) and TimeTagger20.

Funding. Air Force Office of Scientific Research (FA2386-20-1-4014); Australian Research Council (CE200100010, DP190101058).

Disclosures. The authors declare no conflicts of interest.

Data availability. Data underlying the results presented in this paper are not publicly available at this time but may be obtained from the authors upon reasonable request.

REFERENCES

1. I. Aharonovich, D. Englund, and M. Toth, "Solid-state single-photon emitters," Nat. Photonics **10**, 631–641 (2016).
2. A. W. Elshaari, W. Pernice, K. Srinivasan, O. Benson, and V. Zwiller, "Hybrid integrated quantum photonic circuits," Nat. Photonics **14**, 285–298 (2020).
3. M. Atatüre, D. Englund, N. Vamivakas, S.-Y. Lee, and J. Wrachtrup, "Material platforms for spin-based photonic quantum technologies," Nat. Rev. Mater. **3**, 38–51 (2018).
4. C. Li, N. Mendelson, R. Ritika, Y. Chen, Z.-Q. Xu, M. Toth, and I. Aharonovich, "Scalable and deterministic fabrication of quantum emitter arrays from hexagonal boron nitride," Nano Lett. **21**, 3626–3632 (2021).
5. M. A. Feldman, C. E. Marvinney, A. A. Puretzky, and J. Lawrie, "Evidence of photochromism in a hexagonal boron nitride single-photon emitter," Optica **8**, 1–5 (2021).
6. S. A. Breitweiser, A. L. Exarhos, R. N. Patel, J. Saouaf, B. Porat, D. A. Hopper, and L. C. Bassett, "Efficient optical quantification of heterogeneous emitter ensembles," ACS Photon. **7**, 288–295 (2020).
7. J. Ziegler, R. Klaiss, A. Blaikie, D. Miller, V. R. Horowitz, and B. J. Alemán, "Deterministic quantum emitter formation in hexagonal boron nitride via controlled edge creation," Nano Lett. **19**, 2121–2127 (2019).
8. N. V. Proscia, Z. Shotan, H. Jayakumar, P. Reddy, M. Dollar, A. Alkauskas, M. W. Doherty, C. A. Meriles, and V. M. Menon, "Near-deterministic activation of room temperature quantum emitters in hexagonal boron nitride," Optica **5**, 1128–1134 (2018).
9. F. Hayee, L. Yu, J. L. Zhang, C. J. Ciccarino, M. Nguyen, A. F. Marshall, I. Aharonovich, J. Vučković, P. Narang, T. F. Heinz, and J. A. Dionne, "Revealing multiple classes of stable quantum emitters in hexagonal boron nitride with correlated optical and electron microscopy," Nat. Mater. **19**, 534–539 (2020).
10. N. Mendelson, D. Chugh, J. R. Reimers, T. S. Cheng, A. Gottscholl, H. Long, C. J. Mellor, A. Zettl, V. Dyakonov, P. H. Beton, S. V. Novikov, C. Jagadish, H. H. Tan, M. J. Ford, M. Toth, C. Bradac, and I. Aharonovich, "Identifying carbon as the source of visible single-photon emission from hexagonal boron nitride," Nat. Mater. **20**, 321–328 (2021).
11. C. Jara, T. Rauch, S. Botti, M. A. L. Marques, A. Norambuena, R. Coto, J. E. Castellanos-Águila, J. R. Maze, and F. Munoz, "First-principles identification of single photon emitters based on carbon clusters in hexagonal boron nitride," J. Phys. Chem. A **125**, 1325–1335 (2021).
12. A. Gottscholl, M. Kianinia, V. Soltamov, S. Orlinskii, G. Mamin, C. Bradac, C. Kasper, K. Krambrock, A. Sperlich, M. Toth, I. Aharonovich, and V. Dyakonov, "Initialization and read-out of intrinsic spin defects in a van der Waals crystal at room temperature," Nat. Mater. **19**, 540–545 (2020).
13. N. Chejanovsky, A. Mukherjee, J. Geng, Y.-C. Chen, Y. Kim, A. Denisenko, A. Finkler, T. Taniguchi, K. Watanabe, D. B. R. Dasari, P. Auburger, A. Gali, J. H. Smet, and J. Wrachtrup, "Single-spin resonance in a van der Waals embedded paramagnetic defect," Nat. Mater. **20**, 1079–1084 (2021).
14. H. L. Stern, J. Jarman, Q. Gu, S. E. Barker, N. Mendelson, D. Chugh, S. Schott, H. H. Tan, H. Sirringhaus, I. Aharonovich, and M. Atatüre, "Room-temperature optically detected magnetic resonance of single defects in hexagonal boron nitride," arXiv:2103.16494 (2021).
15. J. Liu, R. Su, Y. Wei, B. Yao, S. F. da Silva, Y. Yu, J. Iles-Smith, K. Srinivasan, A. Rastelli, J. Li, and X. Wang, "A solid-state source of strongly entangled photon pairs with high brightness and indistinguishability," Nat. Nanotechnol. **14**, 586–593 (2019).
16. X. Ding, Y. He, Z. C. Duan, N. Gregersen, M. C. Chen, S. Unsleber, S. Maier, C. Schneider, M. Kamp, S. Höfling, C.-Y. Lu, and J.-W. Pan, "On-demand single photons with high extraction efficiency and near-unity indistinguishability from a resonantly driven quantum dot in a micropillar," Phys. Rev. Lett. **116**, 020401 (2016).
17. W. B. Gao, A. Imamoglu, H. Bernien, and R. Hanson, "Coherent manipulation, measurement and entanglement of individual solid-state spins using optical fields," Nat. Photonics **9**, 363–373 (2015).
18. S. Wehner, D. Elkouss, and R. Hanson, "Quantum internet: a vision for the road ahead," Science **362**, eaam9288 (2018).
19. C. Clear, R. C. Schofield, K. D. Major, J. Iles-Smith, A. S. Clark, and D. P. S. McCutcheon, "Phonon-induced optical dephasing in single organic molecules," Phys. Rev. Lett. **124**, 153602 (2020).
20. J. M. Zajac and S. I. Erlingsson, "Temperature dependency of resonance fluorescence from InAs/GaAs quantum dots: dephasing mechanisms," Phys. Rev. B **94**, 035432 (2016).
21. T. T. Tran, M. Kianinia, M. Nguyen, S. Kim, Z.-Q. Xu, A. Kubanek, M. Toth, and I. Aharonovich, "Resonant excitation of quantum emitters in hexagonal boron nitride," ACS Photon. **5**, 295–300 (2018).
22. K. Konthasinghe, C. Chakraborty, N. Mathur, L. Qiu, A. Mukherjee, G. D. Fuchs, and A. N. Vamivakas, "Rabi oscillations and resonance fluorescence from a single hexagonal boron nitride quantum emitter," Optica **6**, 542–548 (2019).
23. B. Spokoyny, H. Utzat, H. Moon, G. Grosso, D. Englund, and M. G. Bawendi, "Effect of spectral diffusion on the coherence properties of a single quantum emitter in hexagonal boron nitride," J. Phys. Chem. Lett. **11**, 1330–1335 (2020).
24. H. Akbari, W.-H. Lin, B. Vest, P. K. Jha, and H. A. Atwater, "Temperature-dependent spectral emission of hexagonal boron nitride quantum emitters on conductive and dielectric substrates," Phys. Rev. Appl. **15**, 014036 (2021).
25. S. J. U. White, N. M. H. Duong, A. S. Solntsev, J.-H. Kim, M. Kianinia, and I. Aharonovich, "Optical repumping of resonantly excited quantum emitters in hexagonal boron nitride," Phys. Rev. Appl. **14**, 044017 (2020).
26. B. Sontheimer, M. Braun, N. Nikolay, N. Sadzak, I. Aharonovich, and O. Benson, "Photodynamics of quantum emitters in hexagonal boron nitride revealed by low-temperature spectroscopy," Phys. Rev. B **96**, 121202 (2017).
27. A. Dietrich, M. Bürk, E. S. Steiger, L. Antoniuk, T. T. Tran, M. Nguyen, I. Aharonovich, F. Jelezko, and A. Kubanek, "Observation of Fourier transform limited lines in hexagonal boron nitride," Phys. Rev. B **98**, 081414 (2018).
28. N. Kalb, A. A. Reiserer, P. C. Humphreys, J. J. W. Bakermans, S. J. Kamerling, N. H. Nickerson, S. C. Benjamin, D. J. Twitchen, M. Markham, and R. Hanson, "Entanglement distillation between solid-state quantum network nodes," Science **356**, 928–932 (2017).
29. L. J. Rogers, K. D. Jahnke, T. Teraji, L. Marseglia, C. Müller, B. Naydenov, H. Schauffert, C. Kranz, J. Isoya, L. P. McGuinness, and F. Jelezko, "Multiple intrinsically identical single-photon emitters in the solid state," Nat. Commun. **5**, 4739 (2014).
30. K. D. Jahnke, A. Sipahigil, J. Binder, M. W. Doherty, M. Metsch, L. J. Rogers, N. B. Manson, M. D. Lukin, and F. Jelezko, "Electron–phonon processes of the silicon-vacancy centre in diamond," New J. Phys. **17**, 043011 (2015).
31. M. Benelajla, E. Kammann, B. Urbaszek, and K. Karrai, "Physical origins of extreme cross-polarization extinction in confocal microscopy," Phys. Rev. X **11**, 021007 (2021).
32. T. Müller, I. Aharonovich, Z. Wang, X. Yuan, S. Castelletto, S. Prawer, and M. Atatüre, "Phonon-induced dephasing of chromium color centers in diamond," Phys. Rev. B **86**, 195210 (2012).
33. V. Hizhnyakov, H. Kaasik, and I. Sildos, "Zero-phonon lines: the effect of a strong softening of elastic springs in the excited state," Phys. Status Solidi B **234**, 644–653 (2002).
34. E. Neu, C. Hepp, M. Hauschild, S. Gsell, M. Fischer, H. Sternschulte, D. Steinmüller-Nethl, M. Schreck, and C. Becher, "Low-temperature investigations of single silicon vacancy colour centres in diamond," New J. Phys. **15**, 043005 (2013).
35. C. Arend, J. N. Becker, H. Sternschulte, D. Steinmüller-Nethl, and C. Becher, "Photoluminescence excitation and spectral hole burning spectroscopy of silicon vacancy centers in diamond," Phys. Rev. B **94**, 045203 (2016).
36. V. Hizhnyakov, V. Boltrushko, H. Kaasik, and I. Sildos, "Strong Jahn–Teller effect in the excited state: anomalous temperature dependence of the zero-phonon line," J. Chem. Phys. **119**, 6290–6295 (2003).
37. V. M. Acosta, C. Santori, A. Faraon, Z. Huang, K. M. C. Fu, A. Stacey, D. A. Simpson, K. Ganesan, S. Tomljenovic-Hanic, A. D. Greentree, S. Prawer, and R. G. Beausoleil, "Dynamic stabilization of the optical resonances of single nitrogen-vacancy centers in diamond," Phys. Rev. Lett. **108**, 206401 (2012).
38. C. P. Anderson, A. Bourassa, K. C. Miao, G. Wolfowicz, P. J. Mintun, A. L. Crook, H. Abe, J. Ul Hassan, N. T. Son, T. Ohshima, and D. D. Awschalom, "Electrical and optical control of single spins integrated in scalable semiconductor devices," Science **366**, 1225–1230 (2019).
39. S. Ates, S. M. Ulrich, S. Reitzenstein, A. Löffler, A. Forchel, and P. Michler, "Post-selected indistinguishable photons from the resonance fluorescence of a single quantum dot in a microcavity," Phys. Rev. Lett. **103**, 167402 (2009).
40. S. Boissier, R. C. Schofield, L. Jin, A. Ovvyan, S. Nur, F. H. L. Koppens, C. Toninelli, W. H. P. Pernice, K. D. Major, E. A. Hinds, and A. S. Clark,

"Coherent characterisation of a single molecule in a photonic black box," Nat. Commun. **12**, 706 (2021).
41. R. Proux, M. Maragkou, E. Baudin, C. Voisin, P. Roussignol, and C. Diederichs, "Measuring the photon coalescence time window in the continuous-wave regime for resonantly driven semiconductor quantum dots," Phys. Rev. Lett. **114**, 067401 (2015).
42. C.-M. Lee, M. A. Buyukkaya, S. Harper, S. Aghaeimeibodi, C. J. K. Richardson, and E. Waks, "Bright telecom-wavelength single photons based on a tapered nanobeam," Nano Lett. **21**, 323–329 (2021).
43. C. Errando-Herranz, E. Schöll, R. Picard, M. Laini, S. Gyger, A. W. Elshaari, A. Branny, U. Wennberg, S. Barbat, T. Renaud, M. Sartison, M. Brotons-Gisbert, C. Bonato, B. D. Gerardot, V. Zwiller, and K. D. Jöns, "Resonance fluorescence from waveguide-coupled, strain-localized, two-dimensional quantum emitters," ACS Photon. **8**, 1069–1076 (2021).
44. N. Nikolay, N. Mendelson, N. Sadzak, F. Böhm, T. T. Tran, B. Sontheimer, I. Aharonovich, and O. Benson, "Very large and reversible stark-shift tuning of single emitters in layered hexagonal boron nitride," Phys. Rev. Appl. **11**, 041001 (2019).
45. G. Noh, D. Choi, J.-H. Kim, D.-G. Im, Y.-H. Kim, H. Seo, and J. Lee, "Stark tuning of single-photon emitters in hexagonal boron nitride," Nano Lett. **18**, 4710–4715 (2018).